PHYSICAL REVIEW B **75**, 020501(R) (2007)

Magnetic switching of phase-slip dissipation in $NbSe_2$ nanoribbons

Abram Falk,[1] Mandar M. Deshmukh,[1] Amy L. Prieto,[2] Jeffrey J. Urban,[2] Andrea Jonas,[2] and Hongkun Park[1,2,*]
[1]*Department of Physics, Harvard University, 12 Oxford Street, Cambridge, Massachusetts 02138, USA*
[2]*Department of Chemistry and Chemical Biology, Harvard University, 12 Oxford Street, Cambridge, Massachusetts 02138, USA*
(Received 26 August 2006; published 3 January 2007)

The stability of the superconducting dissipationless and resistive states in single-crystalline $NbSe_2$ nanoribbons is characterized by transport measurements in an external magnetic field (**H**). Current-driven electrical measurements show voltage steps, indicating the nucleation of phase-slip structures. Well below the critical temperature, the position of the voltage steps exhibits a sharp, periodic dependence as a function of **H**. This phenomenon is discussed in the context of two possible mechanisms: the interference of the order parameter and the periodic rearrangement of the vortex lattice within the nanoribbon.

DOI: 10.1103/PhysRevB.75.020501 PACS number(s): 74.78.Na, 74.40.+k, 74.25.Sv

One-dimensional (1D) superconductors refer to wirelike superconducting materials whose thickness and width are smaller than the Ginsburg-Landau coherence length (ξ) and magnetic penetration depth (λ). These materials have a uniform current distribution over their cross sections,[1] and the onset of resistance in the current (I)-biasing condition is characterized by a sequence of regular voltage (V) steps, corresponding to the nucleation of phase-slip centers (PSCs).[2,3] Recent advances in the synthesis of nanostructured materials have yielded a variety of 1D superconductors, including electrodeposited Pb and Sn nanowires,[4] nanotube-templated amorphous MoGe (Ref. 5) and Nb (Ref. 6) nanowires, laser-ablated $YBa_2Cu_3O_{7-\delta}$ nanowires,[7] and MgB_2 nanowires.[8]

Mesoscopic wires and strips, with one or more dimensions wider than ξ, can also exhibit PSC-like V steps, attributable to Josephson weak-links and spatially extended PSCs.[9] Mesoscopic superconducting wires are also thick enough to support vortices, and thus they provide an interesting model system for investigating the coexistence and the interplay between the PSC-like structures (PSSs) and the Abrikosov vortex lattice.[10] Although mesoscopic $NbSe_2$ films have been used to study single-vortex physics in absence of an applied I,[11] I-driven few-vortex physics has never been investigated in superconducting nanowires.

Here we report transport studies of individual $NbSe_2$ nanoribbons that explore the effect of an external magnetic field on the stability of PSSs. The I-V characteristic of the nanoribbons displays a series of V steps attributable to nucleating PSSs. At low temperatures, the I-V curves become hysteretic. When an external magnetic field (**H**) is applied, the hysteresis sharply decreases for small windows at periodic values of **H**, indicating the switching on and off of phase-slip dissipation caused by thermal activation. We discuss this phenomenon in the context of two possible mechanisms, the interference of the order parameter and the periodic rearrangement of the vortex lattice within the nanoribbon.

Single-crystalline $NbSe_2$ nanoribbons were synthesized by annealing $NbSe_3$ nanoribbons in an inert gas and converting them into $NbSe_2$ nanoribbons.[12] Transmission electron microscopy and x-ray diffraction studies show that the $NbSe_2$ nanoribbons are single crystalline and have a ribbonlike geometry[13] with the c-axis perpendicular to the axis of the nanoribbon (Fig. 1). The thickness (d) and width (w) of typical $NbSe_2$ nanoribbons are $\sim$100 nm.

Devices incorporating individual $NbSe_2$ nanoribbons were fabricated by suspending the nanoribbons in isopropanol, depositing them on a SiO_x or AlN substrate, and contacting

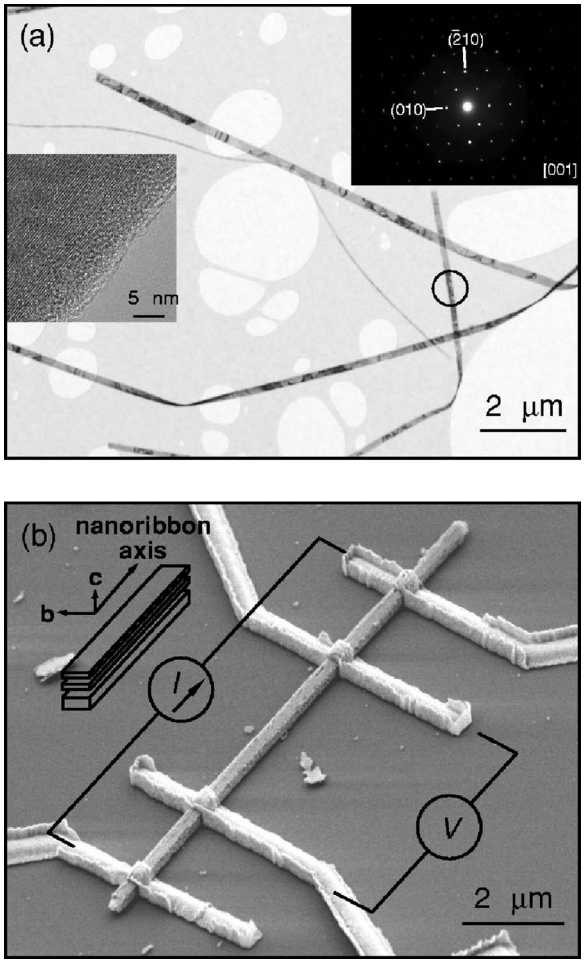

FIG. 1. (a) Transmission electron micrograph of $NbSe_2$ nanoribbons. Inset (left): a high-resolution transmission electron micrograph of a nanoribbon. Inset (upper right): an electron diffraction pattern of the circled nanoribbon. (b) A scanning electron micrograph of a typical four-probe device.

them to bonding pads using conventional electron-beam lithography followed by the sputtering of 60-nm Cr and 200-nm Au layers. Immediately before sputtering, the nanoribbons were cleaned with an Ar plasma in the sputtering chamber. This procedure allows the formation of metal-nanoribbon junctions with low contact resistance (20–100 Ω).

Transport measurements were performed using either a vapor-cooled variable-temperature insert or a 300 mK helium-3 insert in an Oxford Instruments cryostat. The resistance of $NbSe_2$ nanoribbons were measured by I-biasing the nanoribbons with a home-built current source and then measuring the four-probe V. Differential resistance (dV/dI) of the device was also recorded simultaneously, using a lock-in amplifier set at frequency $f=1$ kHz. Measurements on multiple $NbSe_2$ nanoribbon samples showed that the superconducting transition temperature (T_c) of $NbSe_2$ nanoribbons typically ranged between 2 to 2.3 K, lower than bulk values ($T_{c,\mathrm{bulk}}=7$ K).[14] The T_c suppression is most likely caused by disorder, in particular Se impurities resulting from the incomplete conversion of $NbSe_3$ to $NbSe_2$. Previous studies have shown that T_c is very sensitive to stoichiometry [a 5% deviation suppresses T_c from 7 K to 2.2 K (Ref. 14)].

Figure 2(a) shows the basic I-V characteristic of device A at $T=1.7$ K ($T_C=2.1$ K for this nanoribbon). At low I, the V drop across the nanoribbon is small but nonzero and increases with I. As I increases above a switching current (I_{sw}), the first V step appears followed by several more. The I-V curves are reproducible and, at this temperature, nonhysteretic. The linear regions between the V steps roughly extrapolate to a single point, $I_s=4.2\pm0.5$ μA. At high I ($I>40$ μA), the I-V characteristic curves toward the asymptote $V=R_NI$, where R_N is the normal-state resistance of the nanoribbon, indicating that the nanoribbon becomes normal.

The steps in V appear as peaks in dV/dI. Figure 2(b) shows the evolution of these peaks as a function of T. As T increases, the positions of the V steps gradually move inward toward zero current, their width and magnitude soften, and a single I-V step occasionally branches into two distinct steps. These features are symmetric across $I=0$, again confirming the absence of I-V hysteresis at $T\geq1.7$ K.

The inset to Fig. 2(a) shows the I-V characteristic of device A at $T=300$ mK, and shows that hysteresis emerges at lower temperatures. Specifically, the positions of the innermost V step for the I sweep-up (switching current I_{sw}) and sweep-down directions (retrapping current I_r) differ significantly from each other ($I_{sw}>I_r$). Additional V steps also appear in the range $I_{sw}<I<I_r$ during the I down sweep. The device behavior before the first V step is characterized by a dissipationless regime ($0<I<I_c$) and a low-resistance regime ($I_c<I<I_{sw}$). The low-resistance regime is too small to be visible in the Fig. 2(a) inset, but it shows up clearly in Fig. 3.

The investigation of the device I-V characteristics at $T=300$ mK and nonzero $\mathbf{H}$ reveals an intriguing feature that is periodic in $\mathbf{H}$. Specifically, Fig. 3 shows the evolution of dV/dI from device B as a function of $\mathbf{H}$, where $\mathbf{H}\|\mathbf{b}$ (see Fig. 1 for the definition of the crystalline axes). As H is

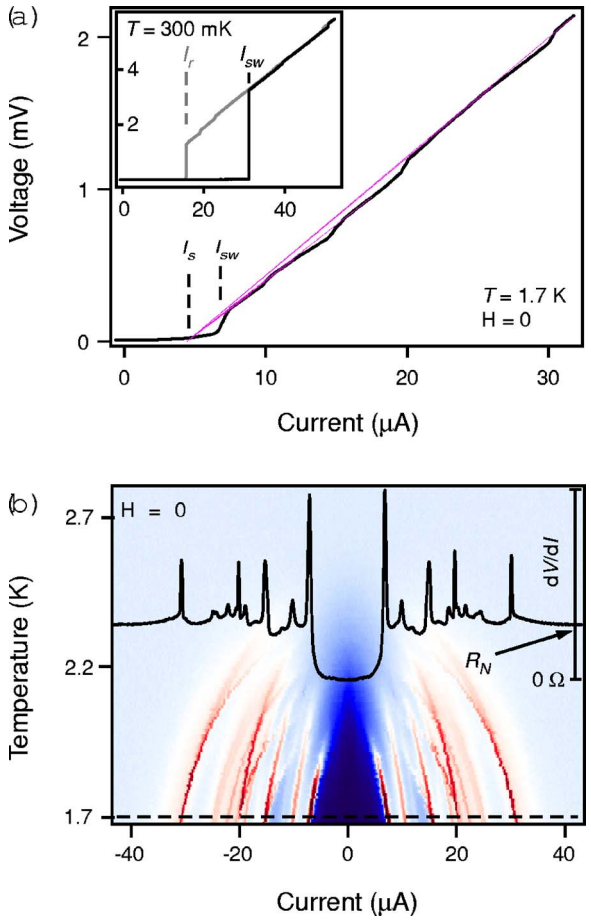

FIG. 2. (Color online) (a) The I-V curve of device A at $T=1.7$ K and $\mathbf{H}=0$. The straight lines are a constrained fit, illustrating how the linear portions of the I-V curve between voltage steps extrapolate to the point I_s. Inset (upper left): The I-V curve of device A at $T=300$ mK and $\mathbf{H}=0$. The dimensions ($w\times d\times$ *inner electrode spacing*) of device A are 130×430 nm$\times10.1$ μm. (b) dV/dI of device A as a function of T and I. The scale is black (0) to gray (R_N) to white. The color scale is purple (0), black, dark blue, light blue (R_N), white, red. The current sweep direction is left-to-right. The line graph is a cross section of dV/dI along the dashed line at $T=1.7$ K.

increased, $I_r(H)$ is periodically enhanced with period $\Delta H=270\pm30$ mT. These enhancements have a finite width, $\delta H=35\pm5$ mT and a binary on-off character, at least within the resolution of our scan (5 mT). The boost to I_r at these values of $\mathbf{H}$ is accompanied by a diminishment to I_{sw}, although the effect of $\mathbf{H}$ on I_{sw} is generally smaller and more varied than its effect on I_r. The other steps do not display the periodic variations, although they do gradually move inward as an increasing $\mathbf{H}$ suppresses the order parameter.

The periodic features illustrated in Fig. 3 were observed in five out of the seven devices that have been measured in detail. Moreover, Fig. 4 shows that these periodic features appear regardless of the $\mathbf{H}$ orientation with respect to the nanoribbon axis, although not every device showed the periodic feature for every orientation of $\mathbf{H}$. Furthermore, the feature only appeared at low temperatures (below 1 K). Comparison of the field scale in Figs. 4(a) and 4(b) indicates that

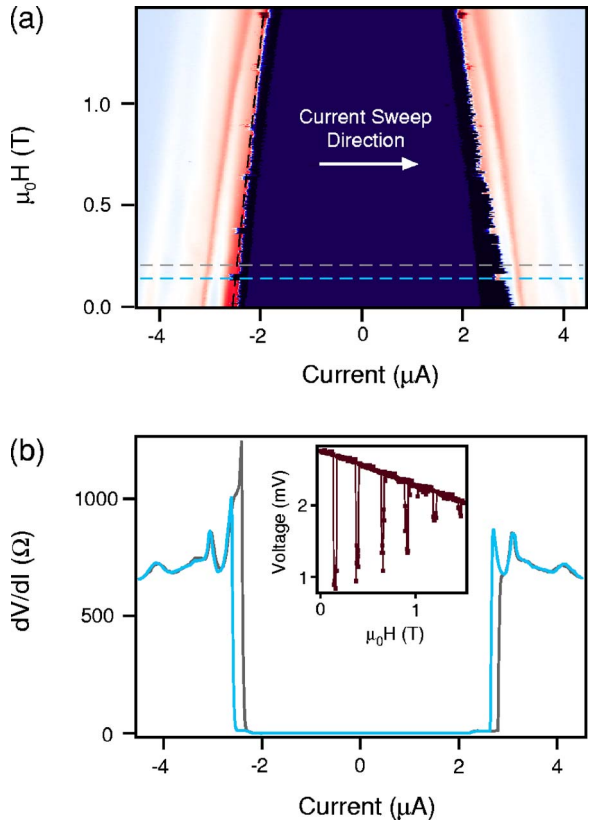

FIG. 3. (Color online) (a) dV/dI of device B plotted as a function of H ($\mathbf{H}\|\mathbf{b}$) and I, at $T=300$ mK. The color scale is the same as Fig. 2(b). (b) Two horizontal cross sections of (a), illustrating the decrease of hysteresis in certain periodic windows of H. Inset: A diagonal cross section of (a) along the dashed line, illustrating the periodic magnetic switching effect. Device B has dimensions 90×530 nm$\times7.3$ μm.

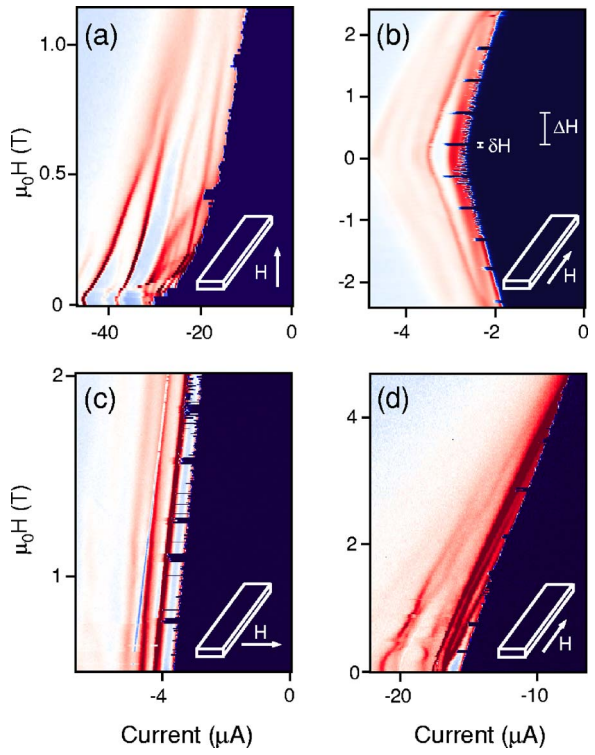

FIG. 4. (Color online) dV/dI plotted as a function of $\mathbf{H}$ and I, at $T=300$ mK, of (a) device A with $\mathbf{H}\|\mathbf{c}$, (b) device B with $\mathbf{H}\|$ nanowire axis, (c) device C with $\mathbf{H}\|\mathbf{b}$, and (d) device D with $\mathbf{H}\|$ nanowire axis. The color scale is the same as Fig. 2(b). The negative I values indicate that I is being swept left-to-right. The dimensions of device C are 60×525 nm$\times3.9$ μm, and device D is 65×375 nm$\times4.8$ μm.

the misalignment of $\mathbf{H}$ with respect to the nanoribbon axis cannot account for the H-periodic features for three different $\mathbf{H}$ orientations. As Fig. 4(b) shows, the evolution of the I-V curves is symmetric about $H=0$ for a given orientation of $\mathbf{H}$.

The V steps in Figs. 2 and 3 are consistent with the nucleation of PSSs observed in low-dimensional superconductors.[3] Specifically, the observation that the linear regions between the voltage steps extrapolate to the point I_s indicates that the V steps observed in $NbSe_2$ nanoribbon devices behave according to the PSC model proposed by Skocpol, Beasley, and Tinkham (SBT).[15] According to the SBT model, the height of the PSC V step is given by

$$V_{\text{step}} = \frac{2\Lambda R_N (I - I_s)}{L},$$

where Λ is the quasiparticle diffusion length that signifies the length scale over which the electrostatic potential and the supercurrent density vary. The fit of the data in Fig. 2 to the SBT model yields $\Lambda\sim4$ μm. Since our $NbSe_2$ nanoribbons are too thick to be truly 1D superconductors, the observed PSSs may have internal structures, such as channels of flowing Abrikosov or kinetic vortices,[16] which arise from the variation of the order parameter over the cross section of the superconductor. We estimate the coherence length of our nanoribbons to be $(\xi_{\perp c}, \xi_{\|c})=(8\text{ nm}, 16\text{ nm})$ at reduced temperature $t=T/T_c=0.6$. These values agree with bulk $NbSe_2$ parameters within our experimental error (the details of this calculation are available online in the EPAPS archive).[14,17,18]

The I-V hysteresis observed in Fig. 3 can be best understood by the theory of underdamped resistively and capacitively shunted Josephson junctions (RCSJ) in the presence of thermal noise.[19] A PSS is a temporal oscillation of the order parameter and thus can be considered as a dynamically generated Josephson junction.[1] While Joule heating likely plays a role in our measurements and contributes to the hysteresis, the fact that I_r enhancements coincided with I_{sw} depressions in our data confirms the importance of the Josephson component to the PSSs. The importance of thermal fluctuations in Josephson junctions is measured by the parameter $\Gamma=k_BT/E_J$, where the Josephson energy E_J is given by $E_J=\hbar I_{sw0}/2e$, and I_{sw0} is the switching current at $T=0$. In the RCSJ model, thermal fluctuations both excite the junction out of the dissipationless state into its resistive state, reducing I_{sw}, and prematurely trap the junction into its dissipationless state, increasing I_r. The periodic feature in our data, which appears as a boost to I_r accompanied by a decrease in I_{sw}, is thus explained by a periodic increase in $\Gamma$with H.

Unfortunately, the experimental data in Figs. 2 and 3 by themselves do not provide a microscopic insight into the underlying cause of the periodic variation in Γ. One possible

mechanism is the interference of the order parameter caused by the magnetic field threading through the PSS, leading to an oscillatory $E_J(H)$ behavior.[20] The matching of vortex rows to the Bean-Livingston surface barrier[21] can also explain such a periodic E_J dip. In this scenario, vortices fill up the thin film row-by-row as H is increased from zero. At certain special values of H called matching fields, a complete chain of in-plane vortices will be filled, and the vortex lattice rearranges to form a new row. If we identify the current at which the vortex lattice becomes unstable with I_{sw0}, then the instability of the vortex lattice corresponds to a minimum in E_J. In principle, Little-Parks oscillation,[22] which causes a periodic dip in $T_c(H)$ in mesoscopic superconductors, might also contribute to the variation in Γ. However, the Little-Parks oscillation cannot account for the periodic $I_r(H)$ features for the $\mathbf{H}\perp$ nanoribbon axis geometries in Fig. 3 and Figs. 4(a) and 4(c), because the Little-Parks oscillation is suppressed for wires and high-aspect ratio rectangles.[23]

In Fig. 4, many of the periodically enhanced I_r windows coincide with the line delineated by another PSS, suggesting that PSS synchronization[6,24] plays a role in explaining the "on-off" nature of the I_r enhancement in periodic windows of H. PSS synchronization can be understood as a heat-mediated interaction between PSSs: the heat generated (lost) by a PSS switching to its resistive (dissipationless) state can trigger a neighboring PSS to switch on (off). The PSS synchronization may only be strong enough to induce switching near a maximum of Γ, thereby explaining the digital character of the $I_r(H)$ effect observed here.

Because the microscopic mechanism for the periodic Γ enhancement remains poorly understood, so does the physical meaning of δH and ΔH. When $\mathbf{H}$ is parallel to the nanoribbon axis, however, it is natural to normalize these quantities to w, d, and the flux quantum ϕ_0, effectively counting the number of vortices that penetrate the nanoribbon. For device B (C) shown in Fig. 4(b) (Fig. 4(d)), the period of the I_r enhancement is $\Delta H = 500 \pm 20$ mT (700 ± 200 mT), corresponding to the addition of ~ 11 vortices, and the width of a single feature is $\delta H = 50 \pm 10$ mT (60 ± 20 mT), corresponding to the addition of 1.0 ± 0.3 vortices. The fact that the normalized δH approximately corresponds to one vortex suggests that single or few vortex processes may play a role in the magnetic switching phenomenon.

The transport study of $NbSe_2$ nanoribbons presented here reveals that the values of I_{sw} and I_r, which measure the stability of the superconducting dissipationless and resistive states, respectively, switch sharply and periodically as functions of H. Our results suggest that superconducting nanoribbons can be an interesting model system for illuminating the interplay between phase-slip dissipation and I-driven vortex physics.

*Author to whom correspondence should be addressed; Electronic address: hongkun_park@harvard.edu

[1] R. Tidecks, Springer Tracts Mod. Phys. **121**, 1 (1990).
[2] W. W. Webb and R. J. Warburto, Phys. Rev. Lett. **20**, 461 (1968); M. Tinkham, J. U. Free, C. N. Lau, and N. Markovic, Phys. Rev. B **68**, 134515 (2003).
[3] J. Meyer and G. v. Minnigerode, Phys. Lett. **38A**, 529 (1972).
[4] S. Michotte, S. Matefi-Tempfli, and L. Piraux, Appl. Phys. Lett. **82**, 4119 (2003); D. Y. Vodolazov, F. M. Peeters, L. Piraux, S. Matefi-Tempfli, and S. Michotte, Phys. Rev. Lett. **91**, 157001 (2003).
[5] A. Bezryadin, C. N. Lau, and M. Tinkham, Nature (London) **404**, 971 (2000).
[6] A. Rogachev and A. Bezryadin, Appl. Phys. Lett. **83**, 512 (2003).
[7] Y. F. Zhang *et al.*, Chem. Phys. Lett. **323**, 180 (2000).
[8] Y. Wu, B. Messer, and P. Yang, Adv. Mater. (Weinheim, Ger.) **13**, 1487 (2001).
[9] A. B. Agafonov *et al.*, Low Temp. Phys. **27**, 686 (2001); A. G. Sivakov *et al.*, Phys. Rev. Lett. **91**, 267001 (2003); J. A. Bonetti, D. S. Caplan, D. J. Van Harlingen, and M. B. Weissmen, *ibid.* **93**, 087002 (2004).
[10] V. M. Dmitriev *et al.*, Low Temp. Phys. **31**, 127 (2005).
[11] C. A. Bolle *et al.*, Nature (London) **399**, 43 (1999).
[12] Y. S. Hor *et al.*, Appl. Phys. Lett. **87**, 142506 (2005); Y. S. Hor *et al.*, Nano Lett. **5**, 397 (2005).
[13] A. L. Prieto, H. Deshmukh, and H. Park (unpublished).
[14] G. A. R. Spiering and E. Beernsten, J. Phys. Chem. Solids **27**, 535 (1966).
[15] W. J. Skocpol, M. R. Beasley, and M. Tinkham, J. Low Temp. Phys. **16**, 145 (1974).
[16] D. Vodolazov, B. J. Baelus, and F. M. Peeters, Physica C **404**, 400 (2004); D. Y. Vodolazov, F. M. Peeters, M. Morelle, V. V. Moshchalcov, Phys. Rev. B **71**, 184502 (2005).
[17] M. J. Higgins and S. Bhattacharya, Physica C **257**, 232 (1996).
[18] See EPAPS Document No. E-PRBMDO-75-R01702 for details of this calculation. For more information on EPAPS, see http://www.aip.org/pubservs/epaps.html.
[19] T. Fulton and L. N. Dunkleberger, Phys. Rev. B **9**, 4760 (1974); M. G. Castellano *et al.*, *ibid.* **54**, 15417 (1996).
[20] R. C. Jaklevic *et al.*, Phys. Rev. Lett. **12**, 159 (1964).
[21] G. Carneiro, Phys. Rev. B **57**, 6077 (1998); Y. Mawatari and K. Yamafuji, Physica C **228**, 336 (1994); T. Yamashita and L. Rinderer, J. Low Temp. Phys. **24**, 695 (1976); M. Ziese, P. Esquinazi, P. Wagner, H. Adrian, S. H. Brongersma, and R. Griessen, Phys. Rev. B **53**, 8658 (1996).
[22] V. V. Moshchalkov *et al.*, Nature (London) **373**, 319 (1995).
[23] G. Teniers *et al.*, Europhys. Lett. **63**, 296 (2003).
[24] D. W. Jillie, J. E. Lukens, and Y. H. Kao, Phys. Rev. Lett. **38**, 915 (1977).